nature neuroscience

Myosin-dependent targeting of transmembrane proteins to neuronal dendrites

Tommy L Lewis Jr[1], Tianyi Mao[2], Karel Svoboda[2] & Don B Arnold[1]

The distinct electrical properties of axonal and dendritic membranes are largely a result of specific transport of vesicle-bound membrane proteins to each compartment. How this specificity arises is unclear because kinesin motors that transport vesicles cannot autonomously distinguish dendritically projecting microtubules from those projecting axonally. We hypothesized that interaction with a second motor might enable vesicles containing dendritic proteins to preferentially associate with dendritically projecting microtubules and avoid those that project to the axon. Here we show that in rat cortical neurons, localization of several distinct transmembrane proteins to dendrites is dependent on specific myosin motors and an intact actin network. Moreover, fusion with a myosin-binding domain from Melanophilin targeted Channelrhodopsin-2 specifically to the somatodendritic compartment of neurons in mice *in vivo*. Together, our results suggest that dendritic transmembrane proteins direct the vesicles in which they are transported to avoid the axonal compartment through interaction with myosin motors.

The differential trafficking of proteins synthesized in the secretory pathway allows the establishment and maintenance of membrane domains with distinct functional and morphological properties at opposite ends of polarized cells[1]. A first step in this process has been well defined in epithelial cells and involves the sorting of proteins at the trans-Golgi membrane into vesicles bound for either the apical or basolateral domain through interaction with clathrin adaptor proteins[2]. In neurons, proteins bound for either the dendritic or axonal domains are also loaded into specific vesicles[3]. Moreover, this sorting step is likely to proceed by a similar mechanism in the two cell types, as AP4β, a constituent of a clathrin adaptor complex, is necessary for dendritic targeting of AMPA receptors[4].

Subsequent steps in polarized targeting of neuronal proteins are much less well defined. However, their properties can be inferred from the observations that vesicles containing dendritic proteins traffic specifically to dendrites, avoiding axonal processes[3], and that kinesin motors, which interact with microtubules, are responsible for movement of vesicles within dendrites[5]. Taken together, these results suggest that after sorting at the Golgi membrane, vesicles carrying dendritic proteins preferentially interact with microtubules that project to dendrites, over those that project to axons. How this choice is made is not known. One possibility is that the kinesin motors that transport vesicles carrying dendritic proteins can distinguish dendritic microtubules from axonal ones. Indeed, dendritic proteins tend to interact with the same kinesin motors, which are often distinct from those kinesins that interact with axonal proteins. For instance, NR2B and Kv4.2, both dendritic proteins, interact with Kif17, a kinesin motor found exclusively in dendrites[6,7]. However, without a cargo, Kif17 cannot distinguish axonal from dendritic microtubules[8], implying that there is a separate mechanism for the selective association of that kinesin motor with dendritic microtubules.

Here we test the hypothesis that vesicles containing dendritic proteins avoid the axonal compartment and accumulate in the somatodendritic compartment as a result of interaction with myosin motors. Previous work has shown that actin is present in the soma and in proximal dendrites in neurons[9] and has implicated myosin motors in protein trafficking to and from dendritic spines in neurons[10–13]. In this report, we present the results of experiments that show that actin and myosin motors are pivotal in dendritic targeting. We show that Myosin Va, a plus-end–directed motor[14], is necessary for targeting of dendritic proteins such as GluR1 and Kv4.2 and that interaction with Myosin Va is sufficient to target nonspecific proteins to dendrites. Moreover, the integrity of actin filaments is necessary for correct targeting of dendritic proteins. Finally, we demonstrate that Channelrhodopsin-2 can be targeted specifically to dendrites in neurons *in vivo* through interaction with Myosin Va, which provides further evidence to support the role of myosin motors in dendritic targeting and establishes a new tool for probing neuronal circuits.

RESULTS

Myosin Va is necessary for dendritic targeting

To investigate possible roles of myosin in polarized targeting, we examined the contributions of Myosins Va and Vb to dendritic targeting of the AMPA receptor GluR1, to which both myosins bind[11,15]. We used dissociated cultures of cortical neurons taken from embryonic day 18 rat embryos and transfected between 12 and 18 d *in vitro* with plasmid constructs encoding tagged transmembrane proteins. When transfected into dissociated rat cortical neurons, GluR1

[1]Department of Biological Sciences and Program in Molecular and Computational Biology, University of Southern California, Los Angeles, California, USA. [2]Janelia Farm Research Campus, Howard Hughes Medical Institute, Ashburn, Virginia, USA. Correspondence should be addressed to D.B.A. (darnold@usc.edu).

Received 3 February; accepted 20 March; published online 19 April 2009; doi:10.1038/nn.2318

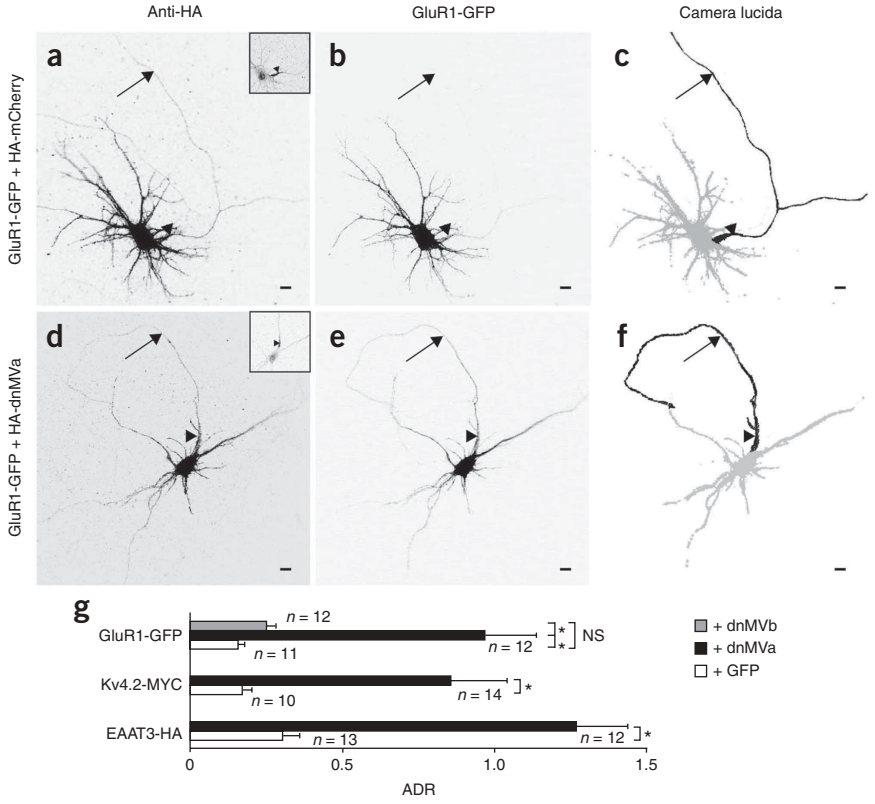

Figure 1 Myosin function is necessary for targeting of exogenous dendritic transmembrane proteins. (**a**–**c**) In a cortical neuron expressing HA-mCherry (**a**), GluR1-GFP (**b**) localized specifically to the somatodendritic region. (**c**) Camera lucida drawing. Axon, black; somatodendritic region, gray. (**d**–**f**) In contrast, when expressed with a dominant negative variant of Myosin Va (HA-dnMVa) (**d**), GluR1-GFP (**e**) localized nonspecifically. (**f**) Camera lucida drawing. (**g**) The axon-to-dendrite ratios (ADRs; see Online Methods) of GluR1-GFP, Kv4.2-MYC and EAAT3-HA expressed with tagged dnMVa were at least fourfold higher than when each was expressed with either HA-mCherry or GFP: $ADR_{GluR1,dnMVa} = 0.97 \pm 0.17$; $ADR_{GluR1,mCherry} = 0.16 \pm 0.02$; $ADR_{KV4.2,dnMVa} = 0.86 \pm 0.19$; $ADR_{Kv4.2,HA\text{-}mCherry} = 0.17 \pm 0.03$; $ADR_{EAAT3\text{-}HA,dnMVa} = 1.27 \pm 0.17$; $ADR_{EAAT3\text{-}HA,HA\text{-}mCherry} = 0.30 \pm 0.05$. Conversely, the ADR of GluR1-GFP was not significantly different when it is expressed with HA-dnMVb ($ADR_{GluR1,dnMVb} = 0.25 \pm 0.03$) from the ADR when it was expressed with HA-mCherry. Error bars, s.e.m.; arrow, axon; arrowheads, axon initial segment. Insets: staining for Ankyrin G, used to identify the axon. Scale bars, 10 μm. $^*P < 0.0002$; NS, $P > 0.08$ (Wilcoxon-Mann-Whitney).

tagged with green fluorescent protein (GFP) (GluR1-GFP) localized specifically to the somatodendritic compartment as expected. (**Fig. 1a–c**)[16]. In each cell examined, the axon was identified by the presence of Ankyrin G, a marker of the axon initial segment, or by the absence of the dendritic marker MAP2 (**Fig. 1a,d**; **Supplementary Fig. 1** online). To block the function of Myosins Va and Vb, we expressed dominant negative variants that contained the tail region, but not the head and neck regions (dnMVa, dnMVb)[17], along with a hemagglutinin (HA) tag. Notably, expression with HA-dnMVa, but not HA-dnMVb, completely disrupted somatodendritic localization of GFP-tagged GluR1 (**Fig. 1d–g**, **Supplementary Fig. 2** online)[16]. Quantitative analysis confirmed these observations: the axon-to-dendrite ratio (ADR; see Methods) of GluR1-GFP when expressed with HA-dnMVa was approximately 1 ($ADR_{GluR1,dnMVa} = 0.97 \pm 0.17$), indicating that the receptor localized with equal efficiency to

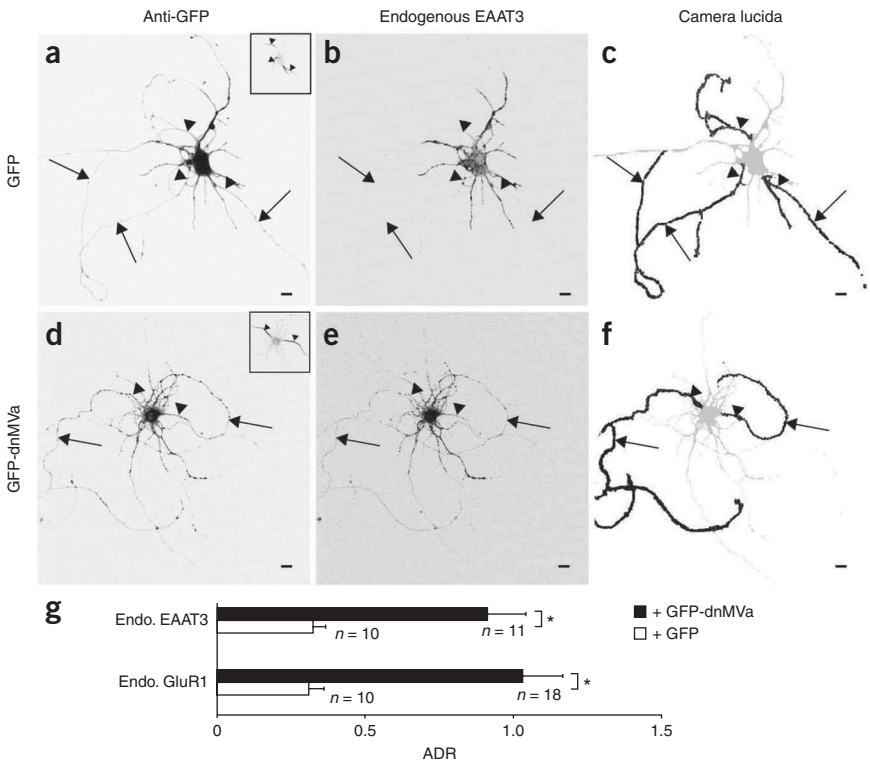

Figure 2 Myosin function is necessary for targeting of endogenous dendritic transmembrane proteins. (**a**–**c**) In a cortical neuron expressing GFP (**a**), endogenous EAAT3 (**b**) localized preferentially to the somatodendritic region. (**c**) Camera lucida drawing. Axon, black; somatodendritic region, gray. (**d**–**f**) In contrast, when expressed with a dominant negative variant of Myosin Va (**d**), endogenous EAAT3 (**e**) localized to both the somatodendritic and axonal compartments. (**f**) Camera lucida drawing. (**g**) The ADRs of endogenous GluR1 and EAAT3 expressed with tagged dnMVa were approximately threefold higher than when each was expressed with either HA-mCherry or GFP: $ADR_{GluR1,dnMVa} = 1.03 \pm 0.13$; $ADR_{GluR1,GFP} = 0.31 \pm 0.05$; $ADR_{EAAT3,dnMVa} = 0.92 \pm 0.13$; $ADR_{EAAT3,GFP} = 0.32 \pm 0.04$. Error bars, s.e.m.; arrow, axon; arrowheads, axon initial segments. Insets, staining for Ankyrin G. Scale bars, 10 μm; $^*P < 0.0009$ (Wilcoxon-Mann-Whitney).

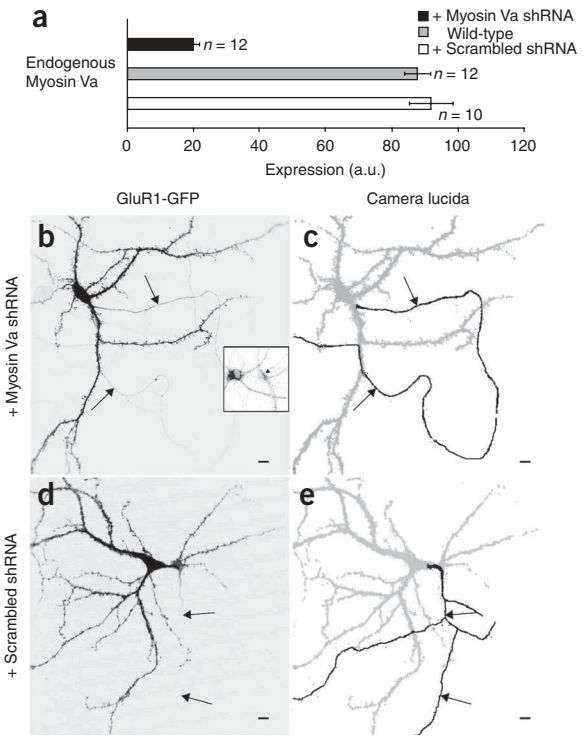

Figure 3 Knockdown of Myosin Va expression blocks dendritic targeting of GluR1-GFP. (**a**) Expression of siRNA directed against Myosin Va in cortical neurons in dissociated culture caused at least a 75% drop in the expression of endogenous Myosin Va ($P < 0.0001$; a.u., arbitrary units). (**b**) Expression of MVa siRNA with GluR1-GFP caused the receptor to localize nonspecifically. (**c**) Camera lucida drawing of neuron shown in **b**. Axon, black; somatodendritic region, gray. (**d**) GluR1-GFP localized to dendrites when expressed with a scrambled siRNA. Inset, staining of endogenous Myosin Va in the neuron shown in **b** (arrowhead) and in an untransfected control. (**e**) Camera lucida drawing of neuron shown in **d**. Error bars, s.e.m.; arrow, axon. The ADR is unnormalized (see Online Methods), so that only the relative values are relevant. Axons were identified by either the presence of Ankyrin G or the absence of MAP2. Scale bars, 10 μm; $^*P < 0.001$ (Wilcoxon-Mann-Whitney).

somatodendritic and axonal compartments. In contrast, when expressed with either HA-mCherry fluorescent protein or with HA-dnMVb, GluR1-GFP was enriched ~4- to 5-fold in the dendritic compartment ($ADR_{GluR1,mCherry} = 0.16 \pm 0.02$; $ADR_{GluR1,dnMVb} = 0.25 \pm 0.03$). Together, these data indicate that Myosin Va is necessary for dendritic targeting of GluR1. We obtained similar results using a dendritic K^+ channel, Kv4.2 (Kv4.2-MYC)[18] and the excitatory amino acid transporter EAAT3 (EAAT3-HA)[19], both of which localized non-specifically when expressed with tagged dnMVa (**Fig. 1g** and **Supplementary Fig. 2**) but somatodendritically when expressed with either HA-mCherry (Kv4.2-MYC) or GFP (EAAT3-HA). To determine whether Myosin Va function was necessary for localization of endogenous proteins, we examined the effect of expressing GFP-dnMVa on localization of endogenous EAAT3 and GluR1. Both proteins were enriched in the somatodendritic compartment in dissociated neurons expressing GFP, as expected (**Fig. 2a–c**). Notably, both proteins were nonspecifically localized in neurons expressing GFP-dnMVa (**Fig. 2d–g; Supplementary Fig. 3** online).

To confirm that Myosin Va function is necessary for dendritic proteins to localize appropriately, we depleted Myosin Va with small interfering RNA (MVa siRNA). In neurons expressing MVa siRNA, both exogenous GluR1-GFP and endogenous GluR1 were nonspecifically localized to both axonal and dendritic compartments (**Fig. 3a–c**; **Supplementary Fig. 4** online). In contrast, both proteins were enriched in dendrites in cells expressing a scrambled siRNA (**Fig. 3d,e**; **Supplementary Fig. 4**). In particular, the ADR of GluR1-GFP expressed with

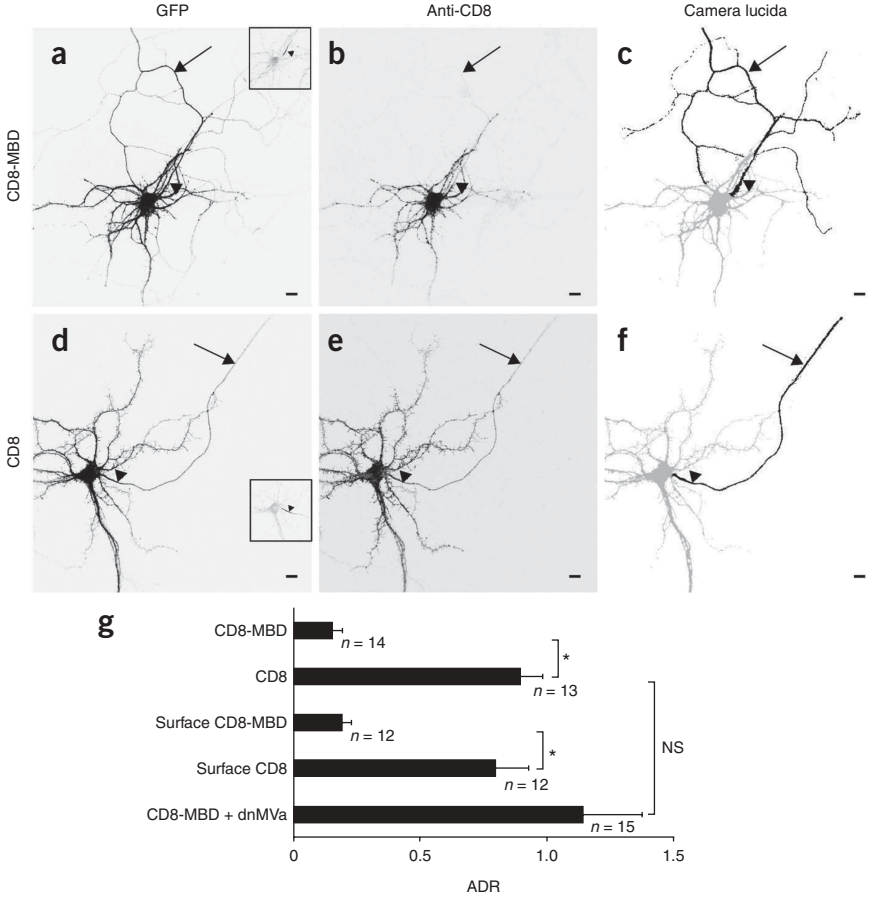

Figure 4 Association with Myosin Va is sufficient for dendritic targeting. (**a–c**) CD8 fused to a Myosin Va binding domain (CD8-MBD) and expressed with GFP in a cortical neuron localized specifically to the soma and dendrites. (**c**) Camera lucida drawing. Axon, black; somatodendritic region, gray. (**d–f**) CD8 expressed with GFP localized to both axons and dendrites. (**f**) Camera lucida drawing. (**g**) CD8-MBD, which associates with Myosin Va, localized dendritically as assessed by either total protein or surface protein staining ($ADR_{CD8\text{-}MBD} = 0.13 \pm 0.02$; $ADR_{CD8\text{-}MBD,surface} = 0.19 \pm 0.04$). In contrast, CD8 localized nonspecifically in either case ($ADR_{CD8} = 0.90 \pm 0.08$; $ADR_{CD8,surface} = 0.80 \pm 0.13$). CD8-MBD localized nonspecifically when expressed with HA-dnMVa ($ADR_{CD8\text{-}MBD,dnMVa} = 1.14 \pm 0.23$). Error bars, s.e.m.; arrow, axon; arrowheads, axon initial segment. Insets, staining for Ankyrin G. Scale bars, 10 μm. $^*P < 0.0002$; NS, $P > 0.08$ (Wilcoxon-Mann-Whitney).

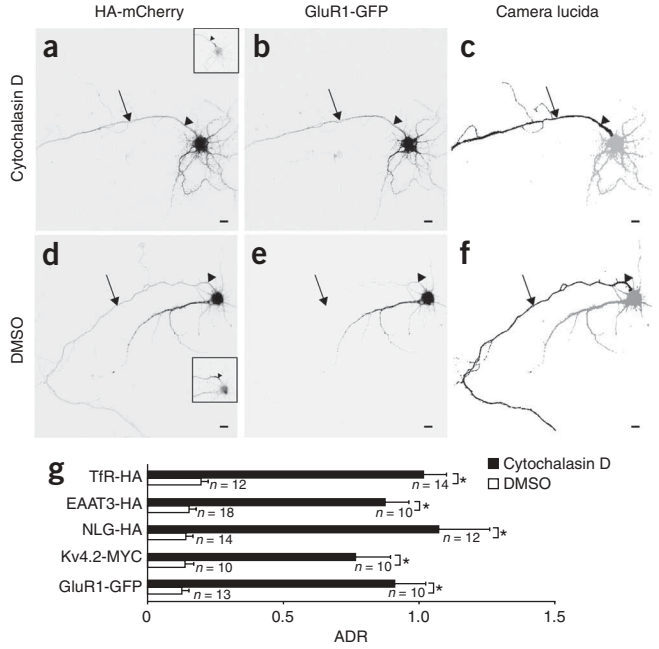

Figure 5 Role of actin in dendritic localization. (**a**–**c**) In a cortical neuron exposed to cytochalasin D for approximately 20 h, both HA-mCherry (**a**) and GluR1-GFP (**b**) localized nonspecifically. (**c**) Camera lucida drawing. Axon, black; somatodendritic compartment, gray. (**d**–**f**) In contrast, in cortical neurons exposed to DMSO, GluR1-GFP expression (**e**) was enriched in the dendrites. (**f**) Camera lucida drawing. (**g**) ADRs confirm that when exogenous dendritic proteins were expressed in cortical neurons exposed to cytochalasin D, they localized nonspecifically ($ADR_{TfR} = 1.01 \pm 0.09$; $ADR_{EAAT3} = 0.87 \pm 0.09$; $ADR_{Nlg} = 1.07 \pm 0.19$; $ADR_{Kv4.2} = 0.76 \pm 0.13$; $ADR_{GluR1} = 0.91 \pm 0.12$), whereas when the same proteins were expressed in similar neurons exposed to DMSO alone, they localized specifically to dendrites ($ADR_{TfR} = 0.20 \pm 0.03$; $ADR_{EAAT3} = 0.15 \pm 0.03$; $ADR_{Nlg} = 0.14 \pm 0.03$; $ADR_{Kv4.2} = 0.14 \pm 0.03$; $ADR_{Glur1} = 0.10 \pm 0.02$). $^*P < 0.0002$ (Wilcoxon-Mann-Whitney); error bars, s.e.m.; arrow, axon; arrowheads, axon initial segment. Insets, staining for Ankyrin G. Scale bars, 10 μm.

MVa siRNA was approximately sevenfold higher than the ADR of the same construct expressed with scrambled siRNA ($ADR_{GluR1,MVa\text{-}siRNA} = 0.22 \pm 0.02$; $ADR_{GluR1,scrambled\text{-}siRNA} = 0.032 \pm 0.005$). The above experiments support the conclusion that Myosin Va function is necessary for dendritic localization of transmembrane proteins. It is unlikely that these results can be attributed to a disruption of myosin-dependent retention of GluR1 in spines, as disruption of spine retention has been shown not to affect polarized targeting[19,20].

Myosin Va is sufficient for dendritic targeting

The above results suggest that myosins are permissive in the localization of dendritic proteins, but is it possible that they are instructive? To address this question, we tested whether a nonspecifically localized protein, CD8, would localize to dendrites when bound to Myosin Va. To bind CD8 to endogenous Myosin Va, we fused it to the Myosin Va binding domain from Melanophilin to give CD8-MBD (ref. 21). After expression in dissociated cortical neurons, CD8-MBD was enriched ~6-fold in dendrites (**Fig. 4a–c**), as compared with CD8 alone (**Fig. 4d–g**).

Dendritic localization of CD8-MBD could not be attributed to a disruption of membrane trafficking, as surface CD8-MBD localized specifically to the somatodendritic region (**Fig. 4g**; **Supplementary Fig. 5** online), in contrast to the nonspecific localization of surface CD8 (**Fig. 4g** and **Supplementary Fig. 5**). To confirm that interaction with Myosin Va was necessary for dendritic localization of CD8-MBD, we expressed it with HA-dnMVa. When expressed with HA-dnMVa, CD8-MBD localized in a nonspecific pattern not significantly different from that of CD8 (**Fig. 4g** and **Supplementary Fig. 5**; $P > 0.6$).

Actin filaments are necessary for dendritic targeting

If myosins are important for localization of dendritic proteins, it would follow that actin would be similarly important. To determine whether actin filaments are necessary for localizing dendritic proteins, we tested the effect of cytochalasin D, which disrupts actin filaments by inhibiting actin polymerization (**Supplementary Fig. 6** online), on the localization of dendritic proteins. In addition to Kv4.2, EAAT3 and GluR1, we also examined Neuroligin 1 (Nlg-HA), a cell adhesion molecule, and the Transferrin receptor (TfR-HA)[22,23]. In neurons treated with cytochalasin D, exogenously expressed TfR, EAAT3, Nlg, GluR1 and Kv4.2 all localized nonspecifically (**Fig. 5a–c**; **Supplementary Fig. 7** online). These results differed significantly from those obtained when the same proteins were expressed in the presence of vehicle (dimethylsulfoxide (DMSO)), wherein ADR measurement indicated a ~5- to 10-fold enrichment in dendrites (**Fig. 5d–g** and **Supplementary Fig. 7**). To verify that these effects were not specific to overexpressed proteins,

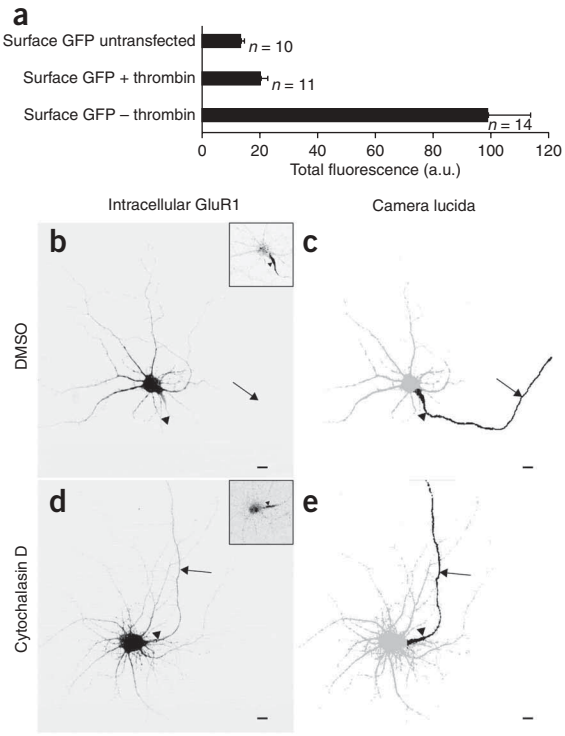

Figure 6 Role of actin filaments in the initial targeting of GluR1 to dendrites. (**a**) In the presence of thrombin, GFP was efficiently cleaved from GluR1-TCS-GFP, which effectively removes the label from all protein that is present on the cell surface, allowing specific labeling of intracellular protein that has never been to the cell surface. The surface staining of GluR1 in the presence of thrombin can largely be attributed to background, as it is similar to the staining seen in neurons that were not transfected. (**b**,**c**) In a cortical neuron exposed to DMSO and thrombin, intracellular GluR1 (**b**) localized specifically to the somatodendritic compartment. (**c**) Camera lucida drawing. Axon, black; somatodendritic compartment, gray. (**d**,**e**) However, in a cell exposed to cytochalasin D and thrombin, intracellular protein localized to both axons and dendrites. Error bars, s.e.m.; Arrow, axon; arrowheads, axon initial segment. Insets, staining for Ankyrin G. Scale bars, 10 μm.

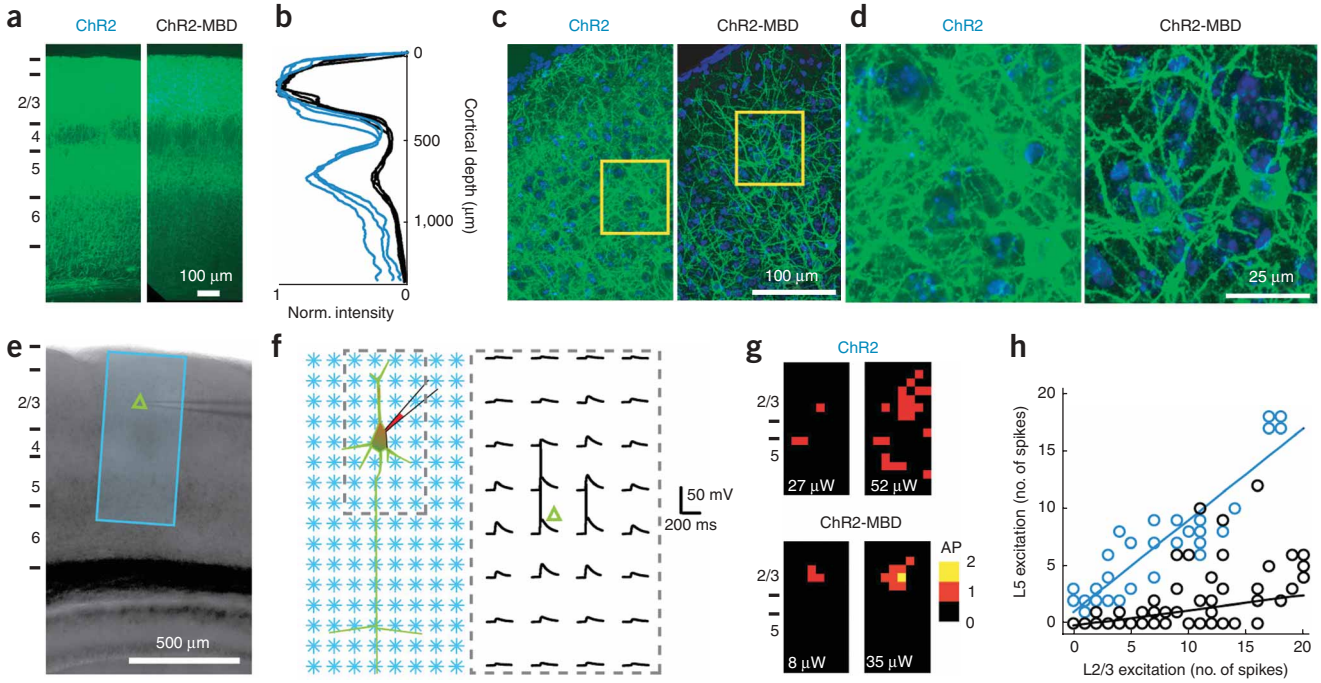

Figure 7 Targeting ChR2 to dendrites of pyramidal neurons using a myosin-binding domain. (**a**) Coronal section through the somatosensory cortex from mice expressing ChR2 (left) and ChR2-MBD (right) tagged with fluorescent proteins in L2/3 pyramidal neurons. Cortical layers are indicated at left. (**b**) Fluorescence intensity normalized to the maximum for each slice (norm. intensity) as a function of cortical depth. (**c**) Confocal images of L2/3 in mice showing expression of ChR2 (left) and ChR2-MBD (right) in green. Blue, DAPI stain showing nuclei. (**d**) Enlargements of regions boxed in **c**. (**e**) Image of a brain slice. Blue box, photostimulation area. Green triangle, position of soma. (**f**) Left, schematic of a L2/3 cell and the photostimulation pattern (16 × 8, 50-µm spacing). Right, traces, recorded in current clamp, corresponding to dashed box on left. (**g**) Excitation profiles of layer 2/3 neurons expressing ChR2 (top) and ChR2-MBD (bottom) at different laser powers (size of stimulation area corresponds to blue box in **e**). AP, action potentials. The ChR2-MBD map at 8 µW corresponds to the data in **f**. (**h**) The number of action potentials in L5 versus L2/3. Data are pooled across cells (ChR2, $n = 9$; ChR2-MBD, $n = 15$) and powers (5–350 µW). Slopes of the regression lines are 0.8 (ChR2) and 0.13 (ChR2-MBD) ($P < 0.001$). In some instances, several points with the same value are plotted on top of each other (**Supplementary Fig. 11**).

we compared the distributions of endogenous Kv4.2, EAAT3 and GluR1 in cells exposed to DMSO versus cytochalasin D. As expected, endogenous Kv4.2, EAAT3 and GluR1 localized somatodendritically in neurons exposed to DMSO but nonspecifically in those exposed to cytochalasin D (**Supplementary Fig. 8** online), indicating that intact actin filaments are necessary for localizing dendritic proteins. Moreover, these results are consistent with experiments showing that exposure of neurons to cytochalasin D for 5 d interferes with differentiation, resulting in the formation of processes that have characteristics of both dendrites and axons[24].

The previous experiments are consistent with roles for actin both in the initial targeting of dendritic proteins as well as in their retention in a polarized distribution. It was previously proposed that actin tethers transmembrane proteins such as sodium channels in the axon initial segment at such a high density that they form a diffusion barrier on the membrane, preventing axonal transmembrane proteins from diffusing out of the axon and dendritic transmembrane proteins from diffusing in[25]. To distinguish between these possibilities, we took advantage of a method for visualizing the distribution of membrane protein before arrival on the cell surface, based on the fusion of the extracellular domain of the protein with GFP upstream of a thrombin cleavage site[26]. We fused GFP to the N terminus of GluR1 (GluR1-TCS-GFP) using a linker containing a thrombin cleavage site (TCS; **Supplementary Fig. 9** online) and transfected the construct encoding the fusion protein into dissociated cortical neurons. Exposure to thrombin in the culture medium caused GFP to be efficiently cleaved from the surface protein (**Fig. 6a**). To examine the effect of actin depolymerization on targeting of GluR1 before its arrival at the plasma membrane, we compared the distribution of GluR1-TCS-GFP in cultures treated with thrombin and either cytochalasin D or vehicle. The distribution of GFP, visualized with antibody staining under permeabilizing conditions, indicated that GluR1 was restricted to the somatodendritic compartment in the presence of DMSO and that this localization was disrupted by cytochalasin D (**Fig. 6b–e**). Comparisons of the unnormalized ADRs (see Methods) of intracellular GluR1 with and without cytochalasin D confirmed these qualitative findings: $ADR_{intracellular\text{-}GluR1+cytochalasin\text{-}D} = 0.29 \pm 0.05$, whereas $ADR_{intracellular\text{-}GluR1+DMSO} = 0.03 \pm 0.009$. These results indicate that an intact actin network is necessary for the initial targeting of GluR1 to dendrites and away from axons, a role that is distinct from the one proposed in the maintenance of these distributions[25].

Dendritic Channelrhodopsin 2: a tool for circuit mapping

In addition to providing a framework for understanding dendritic targeting of transmembrane proteins, the results of the previous experiments suggest a strategy for modifying proteins to target them to dendrites. Expression of Channelrhodopsin-2 (ChR2) is sufficient to produce rapid light-activated cationic photocurrents in heterologous cells[27]. Neurons expressing ChR2 can be entrained to fire precisely timed action potentials in response to brief light pulses[28,29]. In ChR2-assisted circuit mapping, photostimulation of presynaptic neurons is combined with whole-cell recording of putative postsynaptic neurons[30,31]. However, because ChR2 is present in both axons and dendrites, stimulating the somatodendritic region of a given neuron

often also excites colocalized axons, which could originate from distant, functionally unrelated neurons[30]. Axonal expression therefore reduces the utility of ChR2-assisted circuit mapping.

To target ChR2 to dendrites, we fused it with the Myosin Va–binding domain of Melanophilin to give ChR2-MBD. We compared the localization of yellow fluorescent protein (YFP)-tagged ChR2 and YFP-tagged ChR2-MBD in layer (L) 2/3 pyramidal cells in the mouse somatosensory cortex after transfection using *in utero* electroporation[30]. In adolescent mice (postnatal day 23), we found that L5, which contains axons of L2/3 cells, showed roughly 25% of the YFP fluorescence in slices expressing ChR2-MBD as it showed in similar slices expressing ChR2, indicating that ChR2-MBD was excluded from axons (**Fig. 7a**,**b**). Furthermore, confocal images of L2/3 neuropil showed bright dendrites and axons in brains expressing ChR2 but only bright dendrites in brains expressing ChR2-MBD (**Fig. 7c**,**d**). To demonstrate the functional significance of targeting ChR2 to dendrites, we used electrophysiological methods to measure the relative photoexcitability of ChR2 and ChR2-MBD in axons versus dendrites. We recorded from ChR2-expressing neurons in slices of somatosensory cortex using whole-cell or loose-seal patch recordings in the presence of glutamate receptor blockers. Using a blue laser, we stimulated a raster of points overlying layers 1–5 (**Fig. 7e**), and at each location, we determined whether action potentials were evoked for several different stimulation powers (**Fig. 7f**). These excitation maps were highly similar across repetitions (**Supplementary Fig. 10** online). In neurons expressing ChR2, axonal and dendritic locations were roughly equally excitable (**Fig. 7g**, top). For most neurons expressing ChR2-MBD, we could identify a regime of excitation powers where only the dendrites were excitable (**Fig. 7g**, bottom; **Supplementary Figs. 11–14** online). On average, axons in neurons expressing ChR2-MBD were ~1/6 as excitable as axons in neurons expressing ChR2 (**Fig. 7h**). These experiments show that ChR2-MBD was markedly enriched in dendrites compared to axons and suggest that it would be associated with significantly fewer artifacts from spurious axonal stimulation than conventional ChR2. Moreover, they suggest that interaction with Myosin Va can be used to target proteins specifically to dendrites in a manner that does not adversely affect the health and physiological properties of neurons *in vivo*.

DISCUSSION

The experiments in this paper establish for the first time that a common myosin-based mechanism underlies the targeting of dendritic proteins. We show that normal Myosin Va function is necessary for localization of GluR1, Kv4.2 and EAAT3 and demonstrate that interaction with Myosin Va, a plus end–directed motor, is sufficient to mediate dendritic targeting of two otherwise nonspecifically localized proteins. Cytochalasin D, which disrupts actin filaments, causes mislocalization of a variety of dendritic proteins. Together, these results point to a model in which myosin-dependent movement is predominantly in a direction away from the axon and toward the dendrites. Of note, this conclusion is consistent with observations that mitochondria tend to move in a retrograde fashion in axons in the absence of microtubules, when actin-based locomotion prevails[32].

Despite intensive study, the molecular mechanism by which dendritic and axonal proteins are differentially targeted in neurons has remained obscured. Thus, although peptide signals that seem to mediate dendritic targeting have been identified within the amino acid sequences of dendritic proteins[19,22,23,33], this has not provided a mechanistic understanding of the process of polarized targeting. In contrast, some features of the general mechanism underlying trafficking of both axonal and dendritic proteins are well understood. In particular, it is known that proteins bound for specific polarized compartments are carried in distinct vesicles[3,34] and that the movement of these vesicles depends on kinesin motors[35]. The observation from our data that specific targeting of dendritic proteins depends on myosin motors, when combined with the known role of kinesins in trafficking of these proteins, suggests that vesicles containing dendritic proteins interact with both myosin and kinesin motors. This would allow these vesicles to travel along and cross between both actin and microtubule networks. Notably, actin and microtubule networks have been observed to interact—for example, when exposed to microtubule-associated proteins such as MAP2 and MAP1B (refs. 36,37). Indeed, experiments in melanocytes have revealed that vesicles interacting with both motors transition seamlessly from myosin- to kinesin-based movement[38,39].

The observations above are consistent with two models that explain how interaction of actin filaments with microtubules could provide a cytoskeletal track that causes vesicles associated with both a plus end–directed myosin and a kinesin motor to travel to dendrites and avoid axons. In the first model (**Supplementary Fig. 15a** online), vesicles are propelled by myosin motors along actin filaments that are oriented with their plus ends immediately adjacent to dendritic microtubules. After attachment of kinesin motors to these microtubules, the vesicles proceed to dendrites. In the second model (**Supplementary Fig. 15b**), vesicles are initially free to interact with either dendritic or axonal microtubules but are plucked from axonal microtubules when their myosin motors interact with actin filaments in the axon initial segment whose plus ends face toward the cell body. The net effect of such a mechanism would be to prevent vesicles from moving beyond the axon initial segment and, by extension, to bias vesicle movement toward the dendrites. Two observations support the existence of such an axonally based mechanism: (i) when dendritic proteins are expressed in dissociated neurons, they are present in the axon initial segment (**Figs 1–5**); and (ii) their abundance in axons, as reflected by the associated fluorescence, is attenuated with increasing distance from the soma in a myosin-dependent manner (**Supplementary Fig. 16** online). Although it is possible that, in addition to preventing vesicles from moving into the distal axon, actin filaments might facilitate interaction with dendritic microtubules, our results suggest that such a mechanism is imperfect, resulting in at least some accumulation of dendritic proteins in the axon initial segment. Of note, an actin-based structure has been found that creates a region of decreased mobility for transmembrane proteins and prevents axonal and dendritic proteins that are present on the plasma membrane from crossing from one domain to the other[25]. The results reported here would indicate that, in addition to maintaining the polarized distribution of proteins inserted in the membrane, actin-based structures in the axon initial segment are critical in preventing dendritic proteins from reaching the axonal compartment during the initial phase of targeting. In particular, experiments done using cleavable tags (**Fig. 6**) indicate that actin filaments are necessary for the steps in targeting that occur before the nascent protein is deposited on the plasma membrane.

Our results suggest that interaction with plus end–directed motors such as Myosin Va prevent vesicles carrying dendritic proteins from entering axons. How then can this be reconciled with the observation that Myosin Va associates with vesicles that contain presynaptic (axonal) proteins such as SV2, in addition to associating with dendritic proteins[40]? A similar paradox involves the localization of dynein, a minus end–directed microtubule-based motor, throughout the length of the axon despite the predominance of microtubules with minus ends projecting away from the distal axon[41]. It has been explained by the observation that myosin motors drive these dynein complexes anterogradely down the axon[42]. Myosin Va–containing synaptic vesicles

could be transported by similar motors or by plus end–directed kinesins. However, a mechanism must exist to prevent Myosin Va from interacting with actin filaments that project out of the axon. One possibility is suggested by the dynamic nature of Myosin Va, which is regulated by interaction with the vesicle cargo[43] and by phosphorylation[44], as well as by intracellular Ca^{2+}, which binds to associated light chains[14,45]. Thus, Myosin Va could be inactivated during its passage through the axon initial segment and subsequently reactivated to assist in travel through actin-rich regions such as the axon terminals. In the future, it will be important to examine whether Myosin Va function is differentially modulated during different phases of transit through the axon and, if so, by what mechanisms.

Our experiments with ChR2 indicate that association with Myosin Va can target membrane proteins to dendrites. The dendritically targeted version of ChR2 (ChR2-MBD) will be particularly useful for probing spatial aspects of neuronal connectivity. Application of wild-type ChR2 for circuit mapping has been limited because it localizes equally well to axons and to dendrites[30]. As a result, it is virtually impossible to stimulate dendrites from ChR2-expressing cells without also stimulating neighboring ChR2-positive axons; because axonal arbors can be very large, the stimulated axons might arise from distant and functionally unrelated neurons[46]. Axonal photoexcitability therefore degrades the spatial resolution of ChR2 mapping. ChR2-MBD is more than fivefold enriched in dendrites. As a consequence, only neurons with dendrites in the vicinity of the light stimulus will be stimulated, allowing the location of the stimulated cell to be determined. The use of ChR2-MBD will thus greatly facilitate the mapping of neuronal circuits. ChR2-MBD will also improve the spatial resolution of CHR2-mediated microstimulation *in vivo*[47].

In conclusion, the results presented in this paper suggest that a newly recognized mechanism involving myosin motors and actin networks underlies the targeting of dendritic proteins. Although these studies have immediate relevance to the targeting of dendritic transmembrane proteins in neurons, we believe that similar interactions between actin- and microtubule-based networks are likely to be important for the subcellular targeting of a variety of proteins in many cell types.

METHODS

cDNA constructs. TfR-HA was constructed from TfR-GFP (a gift from G. Banker; see Acknowledgments) by replacing the sequence encoding GFP with the sequence encoding a double HA tag. EAAT3-HA was generated by inserting the sequence encoding amino acids 2–525 upstream of a sequence encoding a double HA tag. JPA5 CD8 (G. Banker) was altered by inserting an *Xba*I site and stop codon after amino acid 227. CD8-MBD was constructed by inserting the sequence encoding Melanophilin residues 176–201 into the *Xba*I site. dnMVa-GFP/HA was made by inserting the sequence encoding amino acids 1006–1828 of rat Myosin Va upstream to the sequence encoding EGFP or HA. dnMVb-HA is the sequence encoding amino acids 1221–1846 of rat myosin Vb inserted upstream of the sequence encoding a double HA tag. ChR2-MBD was constructed by inserting the sequence encoding Melanophilin amino acids 176–201 downstream of the *Venus* gene in the CAG-ChR2-Venus vector. Plasmids encoding NLG-HA (M. Silverman) and GluR1-GFP (R. Malinow) were gifts. The thrombin cleavage site, in GluR1-TCS-GFP, was inserted between the cDNAs encoding GFP and GluR1 using a PCR primer encoding the amino acids LVPRGS. Kv4.2-MYC was previously constructed[33]. The siRNA vectors for myosin Va and its scrambled counterpart were gifts from J. Esteban. All constructs were confirmed by DNA sequencing.

Dissociated cultures. Briefly, we removed embryonic day 18 embryos and dissected the cortices in Hanks balanced salt solution (Invitrogen) supplemented with 1 mM HEPES (Invitrogen). Cortices were dissociated in HBSS plus HEPES with 0.25% trypsin for 15 min and then washed three times for 5 min each with HBSS plus HEPES. The dissociated neurons were then plated on coverslips (22 mm × 22 mm, Fisher) at a density of 1×10^4 or 5×10^4 cells per well in neurobasal medium (Invitrogen) supplemented with 10 ml l^{-1} Glutamax (Invitrogen), 1 μg ml^{-1} gentamicin (Invitrogen), 20 ml l^{-1} B-27 supplement (Invitrogen) and 50 ml l^{-1} fetal bovine serum (Invitrogen). After 4 h, the medium was replaced with serum-free neurobasal medium. All cells were transfected using CalPhos (Clontech) at 12–18 d *in vitro* using the manufacturer's suggested protocol. For exogenous proteins, dnMVa was expressed for 16 h, whereas for endogenous proteins, it was expressed for 6 d. Experimental protocols were conducted according to the US National Institutes of Health guidelines for animal research and were approved by the Institutional Animal Care and Use Committee at the University of Southern California.

Cytochalasin D treatment. Two hours after transfection, we added cytochalasin D (Sigma) in DMSO to a final concentration of 1 μM and waited for 16 h before applying fixative. DMSO was present at 0.001% of the final volume.

Immunocytochemistry. The cells were fixed with 4% paraformaldehyde for 5 min and washed with PBS. This was followed by blocking with 1% bovine serum albumin, 5% normal goat serum, 0.1% Triton X-100 in PBS. After blocking, primary antibody was diluted in blocking solution and added for 30–120 min. Secondary antibody was diluted in blocking solution and added for 30 min in the dark. Primary antibody concentrations were as follows: chicken anti-GFP (Aves) 1:1,000, rabbit anti-GFP (BD Biosciences) 1:1,000, mouse anti-HA (Covance) 1:500, rabbit anti–Ankyrin G (Santa Cruz) 1:1,000, mouse anti-CD8 (Dako) 1:100, chicken anti-MYC 1:400 (Aves), mouse anti-Kv4.2 1:20 (Neuromab), rabbit anti-Myosin Va 1:500 (Sigma), rabbit anti-GluR1 1:100 (gift from R. Wenthold; see Acknowledgments), rabbit anti-EAAT3 1:500 (gift from S. Amara), mouse anti-MAP2 1:4,000 (Sigma) and chicken anti-MAP2 (Abcam) 1:12,500. Secondary antibodies were conjugated to Alexa 488, 594 or 647 fluorophores (Invitrogen). Phalloidin 488 (Molecular Probes) was added at the same time as the secondary antibodies.

Surface immunocytochemistry. Fresh neurobasal medium without serum and with primary antibody added was placed on the cells for 60–120 min. The cells were then treated as stated in the immunocytochemistry section.

Thrombin treatment. Neurons were transfected as stated above with GluR1-TCS-GFP. After 8 h, the cells were rinsed twice with buffer (140 mM NaCl, 5 mM KCl, 1 mM $MgCl_2$, 24 mM D-glucose, 10 mM HEPES, 1 mM $CaCl_2$, pH 7.4) and placed into conditioned neurobasal medium. At this time, the medium was supplemented with either DMSO or cytochalasin D and either water or Thrombin (Sigma) at 1 unit ml^{-1}. After 16 h, the neurons were stained as stated in the previous sections.

siRNA experiments. Neurons were transfected as stated above with either MVa or scrambled siRNA vectors and GluR1-GFP. For endogenous experiments, the neurons were transfected with HA-mCherry and either MVa or scrambled siRNA vectors. After 16 h, the cells were rinsed twice with NaCl HEPES buffer and placed into conditioned neurobasal medium for 5 d. On the sixth day, the cells were fixed and stained as stated in the immunocytochemistry section above.

Image capture and analysis. All imaging for **Figures 1–6** was done on a Bio-Rad MRC-1024 confocal microscope. Each cell was imaged as a single optical section. Each image was taken with a ×40 objective and at ×1 zoom. None of the images used for quantification contained any saturated pixels in the axon or dendrites. Cells that had clearly definable axons and overall healthy morphology and were not obscured by neighboring cells were chosen on the basis of GFP or mCherry staining. Axons were identified either by staining of endogenous ankyrin in the initial segment or by the lack of endogenous MAP2 in the axon.

To quantify the degree of polarization in the distribution of a particular protein (P1), we calculated the ADR or axon to dendrite ratio. We calculated two different forms of ADR, normalized and unnormalized. In both cases, we calculated the mean amount of fluorescence per pixel in the entirety of the dendrites and in the axon distal to the initial segment (with background is subtracted from both). We then calculated the ratio of these values to give

an unnormalized ADR, which for most nonspecifically localized proteins was somewhere between 0.2 and 0.3.

$$ADR_{unnormalized=F_{P1,axon}/F_{P1,dendrite}}$$

where $F_{P1,axon}$ is the average fluorescence intensity per pixel of protein P1 in the axon.

For normalized ADR, we then divided by the ratio of the mean fluorescence per pixel in the axon to the mean fluorescence in the dendrites of a nonspecifically localized protein such as GFP.

$$ADR_{normalized} = ADR_{unnormalized}/(Fm_{GFP,axon}/Fm_{GFP,dendrite})$$

where $Fm_{GFP,axon}$ and $Fm_{GFP,dendrite}$ are the amounts of fluorescence associated with GFP in the axon or dendrite, respectively.

The advantage of calculating the normalized ADR is that it is simple to interpret, as ADR = 1 indicates a protein is nonspecifically localized, ADR < 1 indicates a dendritically localized protein and ADR > 1 indicates an axonally localized protein. When a protein was expressed with GFP-dnMVa, it was used to normalize the ADR. GFP-dnMVa localizes nonspecifically, as indicated by an ADR of 1.05 ± 0.08, when compared with mCherry and thus is appropriate for normalization.

All measurements were done using ImageJ (US National Institutes of Health). All values of ADR were expressed ± the s.e.m. Comparisons of ADRs were made with the Wilcoxon-Mann-Whitney test, which can test the significance of nonparametric data. All analyses were performed blinded.

***In utero* electroporation.** Experimental protocols were conducted according to the US National Institutes of Health guidelines for animal research and were approved by the Institutional Animal Care and Use Committee at Janelia Farm Research Campus.

Layer 2/3 pyramidal neurons in the barrel cortex were transfected using *in utero* electroporation. The plasmids for electroporation contained ChR2 fusion proteins (2 μg μl^{-1}). In the case of ChR2-mVenus, cytoplasmic mCherry was co-electroporated at 3:1 molar ratio[30].

Electrophysiology and photostimulation. We used postnatal day 15–23 mice. Recordings in brain slices were as described[30] in the presence of glutamate receptor antagonists (CPP, 5 μM; NBQX, 10 μM). The resting potentials of ChR2-MBD-positive cells, ChR2-MBD-negative cells in the same slices, and ChR2 positive cells were indistinguishable (ChR2-MBD-positive, −66 ± 5 mV, $n = 4$; ChR2-MBD-negative, –66 ± 6 mV, $n = 4$; ChR2, –70 ± 5 mV, $n = 9$). Photostimulation light (473 nm; Crystal Laser; beam diameter, 6 μm, without considering light scattering in the tissue) was delivered through an air immersion objective (×4, 0.16 numerical aperture; UPlanApo, Olympus) on a 16 × 8 grid with 50-μm spacing. Photostimuli consisted of light pulses with 1-ms durations and powers in the range 5–1,000 μW at the specimen. Spikes were recorded in whole-cell current clamp or in loose-seal cell-attached mode.

Immunohistochemistry of slices. Electroporated mice were perfused with cold saline and 4% paraformaldehyde (PFA) and fixed overnight. Sixty-micrometer sections were rehydrated in PBS and incubated with antibodies to green fluorescent protein (rabbit anti-GFP, 0.1 mg ml^{-1}, 1:700; Chemicon) overnight at 4 °C. Slices were then incubated with goat secondary antibody conjugated to Alexa 488 (1:500). Sections were mounted on glass slides for confocal imaging.

Analysis of immunofluorescence data. We measured the intensity profile over a ~100-μm-thick band crossing all cortical layers in three slices (**Fig. 7a,b**). Because the measurements were nearly identical, we simply report the average. The intensity profile was smoothed with a 50-point window, corresponding to 57 μm. We measured the peak fluorescence in L2/3 and L5 in slices expressing ChR2 and ChR2-MBD and computed the ratios:

$$R_{ChR2} = (L23/L5)_{ChR2} = 1.4 \quad (1)$$

$$R_{ChR2-MBD} = (L23/L5)_{ChR2-MBD} = 3.9 \quad (2)$$

where L23 and L5 represent the fluorescence intensities in L2/3 and L5, respectively.

To compute the axonal exclusion, it is necessary to correct for the contribution of axonal labeling in L2/3. Confocal images of L2/3 labeled with ChR2-MBD showed that axonal contributions to the fluorescence signal were negligible. We next compared regions of interest of L2/3 labeled with ChR2-MBD and ChR2 at identical densities. We adjusted image contrast so that the brightest 0.001% pixels, all in somatic and dendritic regions, matched. We then compared the mean intensities of the regions of interest. This analysis revealed that 27% of the L2/3 signal in L2/3 labeled with ChR2 originated in axons.

We can then compute the relative axonal exclusion. Definition of variables: D_{23} = the amount of dendritic membrane in L2/3. D_5 = the amount of dendritic membrane in L5. $r_{d,ChR2\text{-}MBD}$ = the brightness per unit of dendritic membrane in neurons labeled with ChR2-MBD. $r_{d,ChR2}$ = the brightness per unit of dendritic membrane in neurons labeled with ChR2-MBD. A_{23} = the amount of axonal membrane in L2/3. A_5 = the amount of axonal membrane in L5. $r_{a,ChR2\text{-}MBD}$ = the brightness per unit length of axon membrane labeled with ChR2-MBD. $r_{a,ChR2}$ = the brightness per unit length of axon membrane labeled with ChR2.

Because *in utero* electroporation targets L2/3 neurons exclusively (>99.5%)[47], $D_5 = 0$. And because the image contrast was tuned so that the brightest pixels in L2/3, corresponding to somatic and dendritic regions, were matched, $r_{d,ChR2\text{-}MBD} = r_{d,ChR2} = r_d$.

In terms of the ratios in equations (1) and (2) above, we can write

$$(D_{23}r_d + A_{23}r_{a,ChR2})/A_5 r_{a,ChR2} = R_{ChR2}$$

$$(D_{23}r_d + A_{23}r_{a,ChR2\text{-}MBD})/A_5 r_{a,ChR2\text{-}MBD} = R_{ChR2\text{-}MBD}$$

We assume that $D_{23}r_d \gg A_{23}r_{a,ChR2\text{-}MBD}$, and thus $(D_{23}r_d + A_{23}r_{a,ChR2\text{-}MBD}) \approx D_{23}r_d$.

Further, we compare the average brightness in L2/3 with both constructs. Axons do not contribute to fluorescence for ChR2-MBD, but they do contribute for ChR2. The ratio of the mean pixel values in L2/3 is then $R_{23} = (D_{23}r_d + A_{23}r_{a,c2v}) = 1.27$.

$$1.27 D_{23} r_d / A_5 r_{a,ChR2} = R_{ChR2}$$

$$D_{23} r\text{-}d / A_5 r_{a,ChR2\text{-}MBD} = R_{ChR2\text{-}MBD}$$

Dividing the two relationships yields

$$r_{a,ChR2\text{-}MBD}/r_{a,ChR2} = R_{ChR2}/(R_{23}R_{ChR2\text{-}MBD}) = 1.4/(3.9.1.27) = 3.6$$

which represents the relative axonal exclusion. The main systematic error is that background fluorescence from the slice was not subtracted, implying that value computed represents a lower bound on the relative axonal exclusion.

Inflection point analysis for neurons expressing ChR2 and ChR2-MBD. To distinguish photostimulated dendritic action potentials from axonal ones, we analyzed the charging phase (**Supplementary Figs. 13,14**). Action potentials initiated in the soma and dendrite should have a characteristic charging phase, reaching the action potential threshold (approximately + 15 mV relative to rest). To define the action potential threshold, we measured the inflection point in the derivative of the voltage trace: the action potential phase was defined as a peak larger than 25 mV ms^{-1}; the charging phase was identified as a derivative peak larger than 0.5 mV ms^{-1}, before the action potential peak. The inflection point was defined as the location of the minimum derivative between the charging peak and the action potential peak in the graph of voltage versus time.

Data in both the text and panels that are associated with **Figure 7** and **Supplementary Figures 11–14** are presented as mean ± s.d.

Note: Supplementary information is available on the Nature Neuroscience website.

ACKNOWLEDGMENTS

The TfR-GFP and JPA5-CD8 (G. Banker, Oregon Health Sciences University), NLG-HA (M. Silverman, Simon Fraser University), GluR1-GFP (R. Malinow, University of California at San Diego) and siRNA vector (J. Esteban, University of Michigan) plasmids and the antibodies to GluR1 (R. Wenthold, US National Institutes of Health–National Institute on Deafness and Other Communication Disorders) and EAAT3 (S. Amara, University of Pittsburgh) were gifts. The authors would like to thank E. Liman, N. Segil, D. McKemy and members of the Arnold lab for comments on the manuscript and S.H. Kwon for creating the illustrations. This work was supported by US National Institutes of Health grants

NS-041963 and MH-071439 to D.B.A. and support from the Howard Hughes Medical Institute to K.S.

AUTHOR CONTRIBUTIONS

D.B.A. and T.L.L. designed and T.L.L. generated chimeric and mutant constructs. D.B.A. and T.L.L. designed and T.L.L. performed experiments to test constructs in dissociated neuronal cultures; K.S. and T.M. designed and performed the slice experiments; D.B.A., T.L.L., T.M. and K.S. analyzed results; D.B.A., T.L.L. and K.S. wrote the paper; and D.B.A. supervised the project.

Published online at http://www.nature.com/natureneuroscience/
Reprints and permissions information is available online at http://npg.nature.com/reprintsandpermissions/

1. Mostov, K., Su, T. & ter Beest, M. Polarized epithelial membrane traffic: conservation and plasticity. *Nat. Cell Biol.* **5**, 287–293 (2003).
2. Folsch, H., Ohno, H., Bonifacino, J.S. & Mellman, I. A novel clathrin adaptor complex mediates basolateral targeting in polarized epithelial cells. *Cell* **99**, 189–198 (1999).
3. Burack, M.A., Silverman, M.A. & Banker, G. The role of selective transport in neuronal protein sorting. *Neuron* **26**, 465–472 (2000).
4. Matsuda, S. *et al.* Accumulation of AMPA receptors in autophagosomes in neuronal axons lacking adaptor protein AP-4. *Neuron* **57**, 730–745 (2008).
5. Setou, M. *et al.* Glutamate-receptor-interacting protein GRIP1 directly steers kinesin to dendrites. *Nature* **417**, 83–87 (2002).
6. Setou, M., Nakagawa, T., Seog, D.H. & Hirokawa, N. Kinesin superfamily motor protein KIF17 and mLin-10 in NMDA receptor-containing vesicle transport. *Science* **288**, 1796–1802 (2000).
7. Chu, P.J., Rivera, J.F. & Arnold, D.B. A role for Kif17 in transport of Kv4.2. *J. Biol. Chem.* **281**, 365–373 (2006).
8. Nakata, T. & Hirokawa, N. Microtubules provide directional cues for polarized axonal transport through interaction with kinesin motor head. *J. Cell Biol.* **162**, 1045–1055 (2003).
9. Kaech, S., Fischer, M., Doll, T. & Matus, A. Isoform specificity in the relationship of actin to dendritic spines. *J. Neurosci.* **17**, 9565–9572 (1997).
10. Nakata, T., Terada, S. & Hirokawa, N. Visualization of the dynamics of synaptic vesicle and plasma membrane proteins in living axons. *J. Cell Biol.* **140**, 659–674 (1998).
11. Correia, S.S. *et al.* Motor protein-dependent transport of AMPA receptors into spines during long-term potentiation. *Nat. Neurosci.* **11**, 457–466 (2008).
12. Osterweil, E., Wells, D.G. & Mooseker, M.S. A role for myosin VI in postsynaptic structure and glutamate receptor endocytosis. *J. Cell Biol.* **168**, 329–338 (2005).
13. Wang, Z. *et al.* Myosin Vb mobilizes recycling endosomes and AMPA receptors for postsynaptic plasticity. *Cell* **135**, 535–548 (2008).
14. Cheney, R.E. *et al.* Brain myosin-V is a two-headed unconventional myosin with motor activity. *Cell* **75**, 13–23 (1993).
15. Lise, M.F. *et al.* Involvement of myosin Vb in glutamate receptor trafficking. *J. Biol. Chem.* **281**, 3669–3678 (2006).
16. Ruberti, F. & Dotti, C.G. Involvement of the proximal C terminus of the AMPA receptor subunit GluR1 in dendritic sorting. *J. Neurosci.* **20**, RC78:1–5 (2000).
17. Mercer, J.A., Seperack, P.K., Strobel, M.C., Copeland, N.G. & Jenkins, N.A. Novel myosin heavy chain encoded by murine dilute coat colour locus. *Nature* **349**, 709–713 (1991).
18. Sheng, M., Tsaur, M.L., Jan, Y.N. & Jan, L.Y. Subcellular segregation of two A-type K+ channel proteins in rat central neurons. *Neuron* **9**, 271–284 (1992).
19. Cheng, C., Glover, G., Banker, G. & Amara, S.G. A novel sorting motif in the glutamate transporter excitatory amino acid transporter 3 directs its targeting in Madin-Darby canine kidney cells and hippocampal neurons. *J. Neurosci.* **22**, 10643–10652 (2002).
20. Das, S.S. & Banker, G.A. The role of protein interaction motifs in regulating the polarity and clustering of the metabotropic glutamate receptor mGluR1a. *J. Neurosci.* **26**, 8115–8125 (2006).
21. Geething, N.C. & Spudich, J.A. Identification of a minimal myosin Va binding site within an intrinsically unstructured domain of melanophilin. *J. Biol. Chem.* **282**, 21518–21528 (2007).
22. West, A.E., Neve, R.L. & Buckley, K.M. Identification of a somatodendritic targeting signal in the cytoplasmic domain of the transferrin receptor. *J. Neurosci.* **17**, 6038–6047 (1997).
23. Rosales, C.R., Osborne, K.D., Zuccarino, G.V., Scheiffele, P. & Silverman, M.A. A cytoplasmic motif targets neuroligin-1 exclusively to dendrites of cultured hippocampal neurons. *Eur. J. Neurosci.* **22**, 2381–2386 (2005).
24. Bradke, F. & Dotti, C.G. Differentiated neurons retain the capacity to generate axons from dendrites. *Curr. Biol.* **10**, 1467–1470 (2000).
25. Winckler, B., Forscher, P. & Mellman, I. A diffusion barrier maintains distribution of membrane proteins in polarized neurons. *Nature* **397**, 698–701 (1999).
26. Passafaro, M. *et al.* Subunit-specific temporal and spatial patterns of AMPA receptor exocytosis in hippocampal neurons. *Nat. Neurosci.* **4**, 917–926 (2001).
27. Nagel, G. *et al.* Channelrhodopsin-2, a directly light-gated cation-selective membrane channel. *Proc. Natl. Acad. Sci. USA* **100**, 13940–13945 (2003).
28. Boyden, E.S., Zhang, F., Bamberg, E., Nagel, G. & Deisseroth, K. Millisecond-timescale, genetically targeted optical control of neural activity. *Nat. Neurosci.* **8**, 1263–1268 (2005).
29. Li, X. *et al.* Fast noninvasive activation and inhibition of neural and network activity by vertebrate rhodopsin and green algae channelrhodopsin. *Proc. Natl. Acad. Sci. USA* **102**, 17816–17821 (2005).
30. Petreanu, L., Huber, D., Sobczyk, A. & Svoboda, K. Channelrhodopsin-2-assisted circuit mapping of long-range callosal projections. *Nat. Neurosci.* **10**, 663–668 (2007).
31. Arenkiel, B.R. *et al.* In vivo light-induced activation of neural circuitry in transgenic mice expressing channelrhodopsin-2. *Neuron* **54**, 205–218 (2007).
32. Morris, R.L. & Hollenbeck, P.J. Axonal transport of mitochondria along microtubules and F-actin in living vertebrate neurons. *J. Cell Biol.* **131**, 1315–1326 (1995).
33. Rivera, J.F., Ahmad, S., Quick, M.W., Liman, E.R. & Arnold, D.B. An evolutionarily conserved dileucine motif in Shal K^+ channels mediates dendritic targeting. *Nat. Neurosci.* **6**, 243–250 (2003).
34. Kaether, C., Skehel, P. & Dotti, C.G. Axonal membrane proteins are transported in distinct carriers: a two-color video microscopy study in cultured hippocampal neurons. *Mol. Biol. Cell* **11**, 1213–1224 (2000).
35. Guillaud, L., Setou, M. & Hirokawa, N. KIF17 dynamics and regulation of NR2B trafficking in hippocampal neurons. *J. Neurosci.* **23**, 131–140 (2003).
36. Pollard, T.D., Selden, S.C. & Maupin, P. Interaction of actin filaments with microtubules. *J. Cell Biol.* **99**, 33s–37s (1984).
37. Dehmelt, L. & Halpain, S. Actin and microtubules in neurite initiation: are MAPs the missing link? *J. Neurobiol.* **58**, 18–33 (2004).
38. Ali, M.Y. *et al.* Myosin Va maneuvers through actin intersections and diffuses along microtubules. *Proc. Natl. Acad. Sci. USA* **104**, 4332–4336 (2007).
39. Kural, C. *et al.* Tracking melanosomes inside a cell to study molecular motors and their interaction. *Proc. Natl. Acad. Sci. USA* **104**, 5378–5382 (2007).
40. Bridgman, P.C. Myosin Va movements in normal and dilute-lethal axons provide support for a dual filament motor complex. *J. Cell Biol.* **146**, 1045–1060 (1999).
41. Baas, P.W., Deitch, J.S., Black, M.M. & Banker, G.A. Polarity orientation of microtubules in hippocampal neurons: uniformity in the axon and nonuniformity in the dendrite. *Proc. Natl. Acad. Sci. USA* **85**, 8335–8339 (1988).
42. Dillman, J.F. 3rd, Dabney, L.P. & Pfister, K.K. Cytoplasmic dynein is associated with slow axonal transport. *Proc. Natl. Acad. Sci. USA* **93**, 141–144 (1996).
43. Li, X.D. *et al.* The globular tail domain puts on the brake to stop the ATPase cycle of myosin Va. *Proc. Natl. Acad. Sci. USA* **105**, 1140–1145 (2008).
44. Pranchevicius, M.C. *et al.* Myosin Va phosphorylated on Ser1650 is found in nuclear speckles and redistributes to nucleoli upon inhibition of transcription. *Cell Motil. Cytoskeleton* **65**, 441–456 (2008).
45. Krementsov, D.N., Krementsova, E.B. & Trybus, K.M. Myosin V: regulation by calcium, calmodulin, and the tail domain. *J. Cell Biol.* **164**, 877–886 (2004).
46. Luo, L., Callaway, E.M. & Svoboda, K. Genetic dissection of neural circuits. *Neuron* **57**, 634–660 (2008).
47. Huber, D. *et al.* Sparse optical microstimulation in barrel cortex drives learned behaviour in freely moving mice. *Nature* **451**, 61–64 (2008).